LETTERS

Oscillatory dependence of current-driven magnetic domain wall motion on current pulse length

Luc Thomas[1], Masamitsu Hayashi[1,2], Xin Jiang[1], Rai Moriya[1], Charles Rettner[1] & Stuart S. P. Parkin[1]

Magnetic domain walls, in which the magnetization direction varies continuously from one direction to another, have long been objects of considerable interest[1]. New concepts for devices based on such domain walls are made possible by the direct manipulation of the walls using spin-polarized electrical current[2,3] through the phenomenon of spin momentum transfer[4,5]. Most experiments to date have considered the current-driven motion of domain walls under quasi-static conditions[6–12], whereas for technological applications, the walls must be moved on much shorter timescales. Here we show that the motion of domain walls under nanosecond-long current pulses is surprisingly sensitive to the pulse length. In particular, we find that the probability of dislodging a domain wall, confined to a pinning site in a permalloy nanowire, oscillates with the length of the current pulse, with a period of just a few nanoseconds. Using an analytical model[13–17] and micromagnetic simulations, we show that this behaviour is connected to a current-induced oscillatory motion of the domain wall. The period is determined by the wall's mass[18] and the slope of the confining potential. When the current is turned off during phases of the domain wall motion when it has enough momentum, the domain wall is driven out of the confining potential in the opposite direction to the flow of spin angular momentum. This dynamic amplification effect could be exploited in magnetic nanodevices based on domain wall motion.

Most studies of current-induced motion of magnetic domain walls (DWs) have been carried out in magnetic nanowires formed from permalloy ($Ni_{81}Fe_{19}$)[6–10], one of the more attractive magnetic materials for nanodevices because of its low magnetic anisotropy and magnetization yet high Curie temperature[19]. Moreover, the electrical current in permalloy is highly spin polarized owing to significant spin-dependent scattering[19]. Experiments using direct currents or long pulses have shown that in permalloy nanowires, DWs move in the direction of the flow of the electrons (that is, opposite to the electrical current direction) when the current density exceeds a threshold value. In the present work we find that DWs can be moved with nanosecond-long current pulses smaller than the d.c. threshold, but that, under these circumstances, the probability that the DW moves oscillates with the length of the current pulse with a period of a few nanoseconds. Moreover, the DW moves in the opposite direction to the flow of spin-polarized electrons.

We study magnetic domain walls in permalloy nanowires, 200 nm wide and 40 nm thick. The wires are composed of two straight sections oriented at 90° to one another, connected by a curved portion with a radius of curvature of ~3 μm (see Fig. 1a). A single DW is formed in the curved region of the nanowire by applying an appropriate sequence of magnetic fields, as described in Methods. The DW position and its form, whether separating domains with magnetization directions pointing away (tail-to-tail, TT) or towards (head-to-head, HH) one another, depends upon this sequence of fields. Magnetic force microscopy reveals that the DW has a vortex structure (Fig. 1b), as expected from micromagnetic simulations for the size and properties of the wire used[20,21].

Three electrical connections are made to the nanowire—labelled c_i ($i = 1, 2, 3$) in Fig. 1a—which are used both to inject current pulses and to measure the resistance of portions of the wire, R_{ij}, between contacts i and j (see Methods). A DW in the nanowire is readily detected, through the phenomenon of anisotropic magnetoresistance, from a slight drop in the wire's resistance due to the transverse component of the DW's magnetization. As illustrated in Fig. 1c, a small drop in wire resistance between the contacts c_1 and c_2, $\Delta R_{12} \approx 0.15\,\Omega$, is observed when a DW is formed between these contacts. The DW can be moved along the wire by a field, and its motion from the lower to the upper side of the contact c_2 monitored from a small increase in R_{12} (Fig. 1c) (and a corresponding decrease

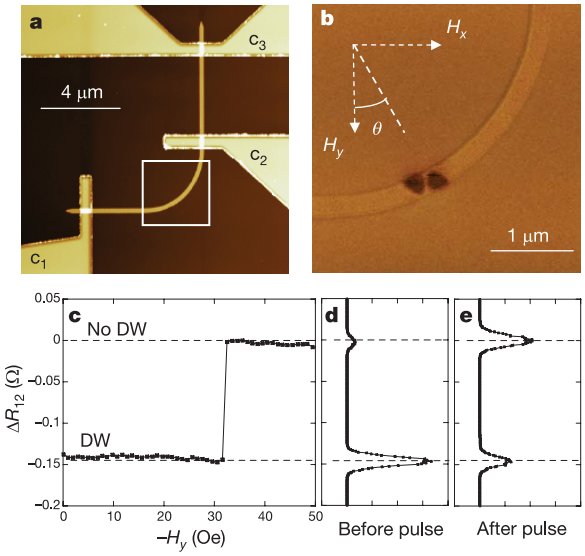

Figure 1 | Experimental configuration. a, Atomic force microscopy image of the device; c_1, c_2 and c_3 are contacts. **b**, Magnetic force microscopy image corresponding to the area enclosed by the white square in **a**. A vortex DW is located in the bend of the wire at a position defined by the angle $\theta \approx 30°$, by using a sequence of in-plane magnetic fields along the two perpendicular directions H_x and H_y. **c**, The change in the wire's resistance between contacts c_1 and c_2, ΔR_{12}, as the HH DW is moved by field $-H_y$ along $-y$ across the contact c_2 without current. Dashed lines depict the wire's resistance with and without a DW. **d**, **e**, Histograms of the resistance levels measured at $H_y = -24$ Oe before (**d**) and after (**e**) the application of a current pulse ($V_p = -2.0$ V, $0.5 < t_p < 30$ ns).

[1]IBM Almaden Research Center, 650 Harry Road, San José, California 95120, USA. [2]Department of Materials Science and Engineering, Stanford University, Stanford, California 94305, USA.

in R_{23}, not shown). At zero current, the magnetic field along y (H_y) required to move the DW from its initial position across c_2 is $\sim\pm36$ Oe for TT and HH DWs, respectively. The DW motion occurs when the component of H_y tangential to the wire at the DW position overcomes local pinning ($\sim$25 Oe), which probably results from edge roughness in the curved portion of the wire.

Current-driven DW motion is explored by first creating a DW in the nanowire and then by injecting a voltage pulse into the wire between contacts c_1 and c_2. Measurements of ΔR_{12} before and after the pulse reveal whether the DW has moved across the contact c_2 (Fig. 1d and e). The probability of DW motion, P_M, is determined as a function of the magnetic field H_y, the voltage pulse amplitude V_p and the pulse length t_p by repeating the same sequence of DW injection and current pulsing 30 times for each set of parameters. Figure 2a–d show P_M for both HH and TT DWs as a function of t_p and H_y, for a constant pulse voltage of $\pm$2.0 V. Both types of DWs exhibit similar behaviours, whereas the dependence of P_M on the pulse length is strongly asymmetric with voltage polarity. DW motion occurs only with a very low probability below a threshold field (for the currents considered in these experiments). For positive voltages (electrons flowing from c_1 to c_2), the threshold field, which varies little with pulse length for pulses longer than $\sim$3 ns, is $\sim$10 Oe and ~-5 Oe for TT and HH DWs, respectively. Above this threshold, P_M increases rapidly to $\sim$100%. On the contrary, for negative voltages, pronounced periodic oscillations of the DW motion probability are observed as the current pulse length is increased for fields ranging from 5 Oe to 30 Oe. The period of the oscillations is $\sim$3 ns and $\sim$4 ns for TT and HH DWs, respectively, but the number of oscillations observed increases with increasing field until the field is so large that the DWs are always depinned, independent of the current pulse length.

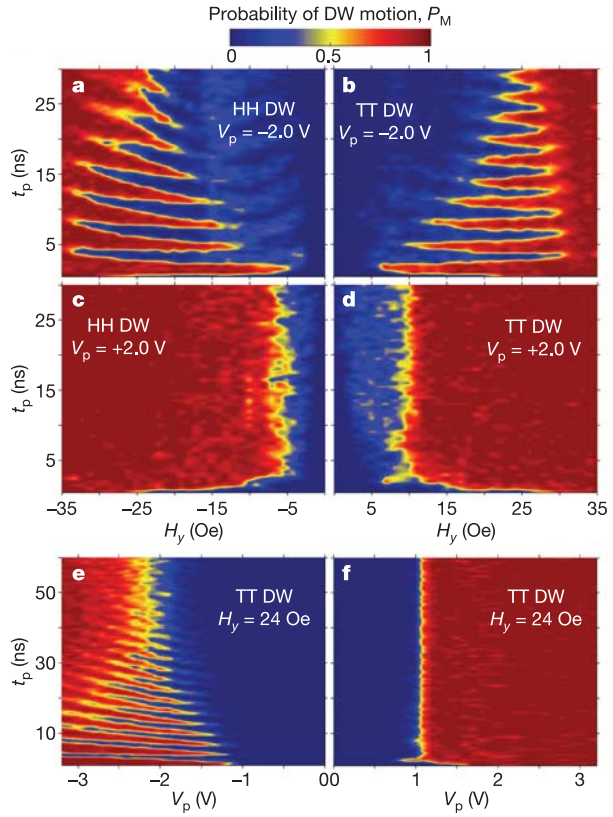

Figure 2 | Probability of motion of a domain wall subjected to current pulses of various lengths and amplitudes. Contour plots of the probability of current-driven DW motion P_M (colour scale) as a function of the current pulse length t_p, the pulse amplitude V_p and the magnetic field H_y ($H_x \approx 0$). Data points are taken every 1 Oe, 0.5 ns and 100 mV. **a**–**d**, Data for varying t_p and H_y at indicated values of V_p for HH (**a**, **c**) and TT (**b**, **d**) DWs; **e**, **f**, Data for varying t_p and V_p at indicated values of H_y. HH and TT stand for head-to-head and tail-to-tail DWs, respectively.

The dependence of P_M on the pulse amplitude and length is shown at a constant field $H_y \approx 24$ Oe for TT DWs in Fig. 2e and f. Again, we observe a strong asymmetry with the pulse polarity. For positive voltages, DW motion occurs above a voltage threshold ($\sim$1 V) that is insensitive to the pulse length. For negative voltages, an oscillatory behaviour is observed. More than 10 oscillations can clearly be identified. The period of these oscillations increases for higher voltages, from $\sim$2.9 ns for $V_p = 1.5$ V, up to $\sim$3.9 ns for 3.2 V. We find that the oscillatory DW depinning is a general phenomenon, which we have observed not only in other permalloy nanowires of various widths ($\sim$100–300 nm) and thicknesses ($\sim$10–40 nm), but also in other materials (for example, FeCoNi) and structures (for example, spin-valve nanowires).

Our results appear consistent with the spin-transfer torque mechanism, in which the transfer of spin angular momentum from a polarized electrical current to the magnetization of the nanowire can induce DW motion[2,3,13–17], although the oscillatory behaviour we observe corresponds to DWs actually moving against the electron flow. Note that any field-related mechanism induced by the current pulse should give rise to opposite voltage polarity dependences for HH and TT DWs, which we do not observe.

We now develop an understanding of the oscillatory DW depinning using the well-established one-dimensional (1D) model[1]. In this model, the profile of the DW is assumed to be unchanged during its motion so that its dynamics can be described by just two parameters, its position and its conjugate momentum. The latter is defined as $2M_S\Psi/\gamma$, where Ψ is the tilt angle of the wall magnetization out of the plane of the wire (see Fig. 3g), M_S is the saturation magnetization ($\sim$800 e.m.u. cm^{-3} for permalloy) and γ is the gyromagnetic factor (17.6 MHz Oe^{-1}). The 1D model has recently been generalized to include a spin-torque term[13–17], so that the Landau–Lifshitz–Gilbert equations of motion become:

$$(1+\alpha^2)\dot{q} = -\frac{\alpha\gamma\Delta}{2M_S}\left(\frac{\partial\varepsilon}{\partial q}\right) + \frac{\gamma\Delta}{2}H_k\sin(2\Psi) + (1+\alpha\beta)u$$

$$(1+\alpha^2)\dot{\Psi} = -\frac{\gamma}{2M_S}\left(\frac{\partial\varepsilon}{\partial q}\right) - \frac{\gamma\alpha}{2}H_k\sin(2\Psi) + (\beta-\alpha)\frac{u}{\Delta}$$

where q and Δ are the DW's position and width, respectively, α is the Gilbert damping parameter, and H_k is the shape anisotropy field in the plane perpendicular to the wire's length that keeps the magnetization in the plane of the wire. The spin torque term is $u = \mu_B JP/eM_S$, with e the electron charge, J the current density, P the polarization of the current, and μ_B the Bohr magneton. When u is positive, the DW is driven in the direction of increasing q. β arises from a non-adiabatic contribution to the spin transfer torque[14–17]. The term $\varepsilon(q)$ is the DW potential energy per unit cross-sectional area, which includes a magnetic field along the DW propagation direction and a pinning potential term. The DW is pinned at a defect in the nanowire. For simplicity, we assume a parabolic potential of depth V and spatial extension q_0 such that, at $H = 0$, $\varepsilon(q) = Vq_0(q/q_0)^2$ for $|q| < q_0$ and $\varepsilon(q) = Vq_0$ for $|q| \geq q_0$.

Let us consider first the simplest case where $\beta = 0$ and $H = 0$. When a current smaller than the d.c. critical depinning current is applied, both q and Ψ oscillate in time (Fig. 3a, b) towards the equilibrium position $(0, \Psi_{eq}(u))$, with an oscillation frequency ω. The DW trajectory in the phase space (q, Ψ) is thus a spiral for which the oscillations are damped according to α (Fig. 3c). However, if the current is cut off before the DW reaches the final equilibrium position, the trajectory of the DW switches to a different orbit centred around the new equilibrium position without current, (0,0), as illustrated in Fig. 3d–f. Depending on the DW's momentum (that is, magnitude of Ψ) when the current is cut off, the amplitude of the oscillations is amplified (red curves in Fig. 3d and f), and the DW can leave the pinning potential. This is remarkable, as the DW is

otherwise pinned for intermediate or longer current pulses. Moreover, the DW leaves in the opposite direction to that when driven by a current larger than the d.c. threshold current. Red lines in Fig. 3a–c show the current pulse cut-off times for which the DW leaves the pinning potential. The oscillation frequency is calculated from the equations of motion using a linear approximation ($\Psi \ll 1$): $\omega \approx \gamma[VH_k\Delta/(M_S q_0)]^{1/2}$. Note that this is simply the resonance frequency of a free harmonic oscillator of mass $m = 2M_S/(\gamma^2 H_k \Delta)$ (that is, the DW mass) in a restoring force $-2V/q_0$ (that is, the slope of the pinning potential). Both the DW mass and the restoring force are normalized per unit cross-sectional area.

In order to validate the results of the 1D model, we have carried out micromagnetic simulations[22] of nanowires with different DW structures, both transverse (Fig. 3g) and vortex (Fig. 3h). Pinning of the DW was mimicked by including a small non-magnetic defect at one edge of the wire (see Methods). The main features found using the 1D model are reproduced for both DW structures. For currents smaller than the critical current, the DW centre oscillates within the potential well around its equilibrium position. The comparison with the 1D model is straightforward for the transverse wall (Fig. 3g). The oscillation in position ($\sim M_x$) is associated with a slight tilt of the magnetization out of the plane of the wire ($\sim M_z$), as described by the conjugate momentum Ψ in the 1D approximation. For DWs with vortex structures (Fig. 3h), the oscillation of the DW within the potential well is associated with a gyrotropic motion of the vortex core, quite similar to the field[23,24] or current driven dynamics[25] of a vortex core confined in a sub-micrometre disk. Magnetization maps of the vortex wall at rest and when distorted during its motion are shown in Fig. 3h. The net magnetization perpendicular to the wire's long axis ($\sim M_y$) oscillates, providing a good measure of the conjugate momentum Ψ. For both DW structures, the DW leaves the potential well only if its momentum is large enough when the current is cut off. Red and black symbols in the lower panels of Fig. 3g and h illustrate the pulse lengths for which the DW is or is not depinned, respectively. Note that the period of the oscillations increases with the dimensions of the nanowire from 0.5 ns (width 100 nm, thickness 5 nm; Fig. 3g) to 3 ns (width 200 nm, thickness 40 nm; not shown) and is in good agreement with the analytical expression calculated from the 1D model.

Micromagnetic simulations exhibit complex dynamical processes beyond the reach of the 1D approximation. For example, the DW structure can be distorted during the current pulse, and thus influence the DW motion. Nevertheless, the 1D model appears to describe well the essential physical mechanisms responsible for the oscillatory dependence of the DW motion on the pulse duration. We now show that this model can be used to describe our experiments quantitatively. Realistic parameters are estimated from micromagnetic calculations (see Methods). Current-driven DW motion is mapped for a TT DW as a function of t_p and H_y at constant u (Fig. 4a and b), and as a function of t_p and u at constant field (Fig. 4c and d). These maps are in good agreement with the experiments. For positive currents (electron flow along the field-driven motion direction), the threshold for depinning the DW is roughly independent of the length of the pulse because the DW leaves the pinning potential during the pulse. On the contrary, for negative currents, depinning occurs after the current is cut off. By fitting the experimental data to this model, we can deduce the

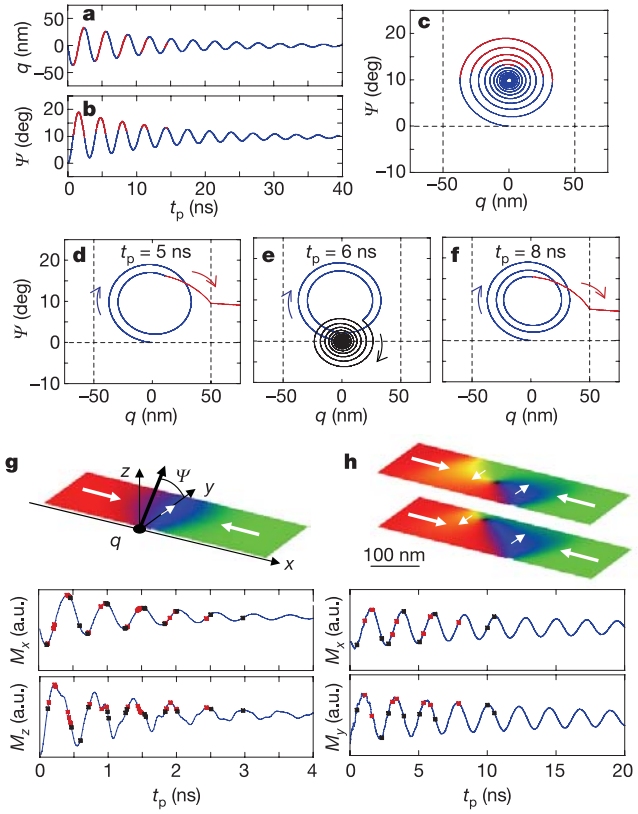

Figure 3 | Current-driven dynamics of a domain wall pinned in a parabolic potential well calculated with the 1D model. The Gilbert damping is $\alpha = 0.005$, the non-adiabatic contribution is $\beta = 0$, and the current parameter $u = -80\ \mathrm{m\,s^{-1}}$; other parameters are described in Methods. Note that thermal effects are not included. **a**–**c**, Time dependence of the DW position q (**a**) and momentum Ψ (**b**) and the DW trajectory in the phase space (q, Ψ) for direct current (**c**). Red lines show the pulse length for which the DW leaves the potential well after the pulse. Vertical dashed lines indicate the width of the potential well (±50 nm). **d**–**f**, Examples of the DW trajectory in phase space for different pulse lengths. **g**, **h**, The bottom panels show colour maps of micromagnetic simulations (at 0 K) of permalloy nanowires with transverse (**g**) and vortex (**h**) DW structures. For the vortex wall (**h**), colour maps are shown at rest (top) and during the gyrotropic motion of the vortex core (bottom). Both nanowires are 100 nm wide, and their thickness is 5 nm (**g**) and 20 nm (**h**). The adiabatic spin transfer torque and the Oersted self-field are included in the simulations ($\beta = 0$). Gilbert damping is $\alpha = 0.01$. Solid lines show the net magnetization components M_x (~DW position), and M_y or M_z (~DW momentum, see text) for a current of 3 mA (current densities of 6.0×10^8 and $1.5 \times 10^8\ \mathrm{A\,cm^{-2}}$, respectively) and a magnetic field $H_x = 10$ Oe. Red and black symbols show whether the DW leaves or remains trapped at the notch after the current is turned off for different pulse lengths.

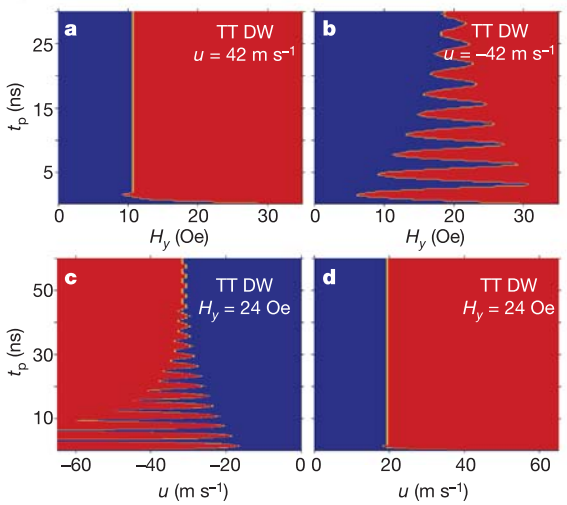

Figure 4 | Contour maps of the domain wall response to current pulses calculated within the 1D model. **a**–**d**, t_p is the pulse length, H_y the magnetic field, and u, the spin-torque parameter (proportional to current). The model parameters are deduced from micromagnetic simulations (see Methods). Regions in which DW motion does or does not occur are shown in red and blue, respectively.

magnitude of the damping constant, $\alpha \approx 0.005$, the non-adiabatic parameter, $\beta \approx 0.04$, and the current polarization, $P \approx 0.4$. The large value of β ($\sim 8\alpha$) suggests that the non-adiabatic spin transfer torque plays a significant role in the current-driven DW motion mechanism[15,16]. Although our model does not account for certain details of our experimental results, such as the different oscillation periods for HH and TT DWs and the voltage dependence of these periods, the model clearly reveals the physical origin of the oscillatory depinning phenomenon.

We have observed an unusual phenomenon in which current-induced DW oscillations are amplified after the end of the current pulse, if the timing of the pulse matches the DW precession period. Taking advantage of this dynamic amplification could open ways of reducing the critical current density needed to move DWs in magnetic nanodevices.

METHODS

Experimental set-up. The nanowire was fabricated by electron-beam lithography from a 40-nm-thick permalloy film grown by magnetron sputtering deposition on a high-resistivity Si wafer. The film was capped with 1 nm TaN/5 nm Ru to prevent oxidation. The nanowire was coated on the sides with Al_2O_3 to limit oxidation along its edges. Another lithographic step was used to fabricate three contact pads (45-nm-thick Rh), labelled c_1, c_2 and c_3 in Fig. 1a. A single DW is formed in the nanowire by first applying a magnetic field of $\sim$700 Oe, larger than the shape anisotropy of the wire, to align the wire's magnetization along a direction tilted at an angle $\theta \approx 85°$ to the wire (Fig. 1b). When this field is reduced to zero, the magnetizations in the wire's two straight sections orient along their respective lengths and a DW is formed in the curved region of the nanowire. In a second step, the DW is moved down and around the bend by applying a field ($\sim$80 Oe) along the y direction ($\theta = 0°$). The form of the DW, whether tail to tail or head to head, depends on whether negative or positive fields are used. The initial position of the DW is then at $\theta \approx 44°$.

Voltage pulses, with rise and fall times of about 0.1 ns, are injected in the nanowire between contacts c_1 and c_2 using a 7 GHz bandwidth probe. The d.c. magnetoresistance of the wire is measured using the same probe through a bias tee. As the change in resistance associated with the DW (ΔR_{12}) is small, the device resistance is compared to a reference state without a DW by making a measurement in zero field after saturating the wire in 700 Oe along $\theta = -60°$. A small d.c. test current ($\sim$0.25 mA) is applied to the sample throughout the measurements. The conversion between the nominal voltage pulse V_p and the actual current pulse I flowing through the device is $I = 2V/(R + Z_0)$, where $R \approx 310\,\Omega$ is the device d.c. resistance between c_1 and c_2 at room temperature (including the contribution of the two contact pads, $\sim 80\,\Omega$) and $Z_0 = 50\,\Omega$ is the characteristic impedance of the transmission line. The current through the device is $\sim 5.5\,\mathrm{mA\,V^{-1}}$, corresponding to a current density of $\sim 6.9 \times 10^7\,\mathrm{A\,cm^{-2}}$. For voltages higher than $\sim$1 V, Joule heating during the pulse causes the device resistance to increase. Time-resolved measurements performed using a sampling oscilloscope show that the device resistance increases by a factor up to 1.3 for the highest pulse voltage used in this study (3.2 V), corresponding to a temperature rise of $\sim$100 K. As the device resistance and the current vary with the pulse length, the pulse amplitude is defined using the nominal output voltage V_p rather than the current.

Determination of the parameters for the 1D model. Realistic values of the DW width parameter Δ and the transverse anisotropy H_k are estimated from micromagnetic simulations of a nanowire (200 nm wide, 40 nm thick) with a vortex DW. We find the dynamical DW width $\Delta \approx 15$ nm, in good agreement with ref. 21. Note that the discrepancy between this very small value and the apparent physical size of the DW (Fig. 1b) results from the strong influence of the vortex core on the DW motion. The transverse anisotropy $H_k = 1{,}800$ Oe is estimated from the Walker breakdown field, above which the DW velocity decreases strongly[1]. The width of the pinning potential, $q_0 = 50$ nm, is obtained by simulating the quasi-static field-driven depinning of the DW from a small non-magnetic defect (10 nm long, 5 nm wide) introduced at one edge of the wire. Note that q_0 is not only determined by the physical size of the pinning defect but also by the DW profile. The magnitude of the pinning potential $V = 2 \times 10^4\,\mathrm{erg\,cm^{-3}}$ is calculated from the formula derived in the text for the oscillation period so as to match the experimental value of $\sim$3 ns.

For the calculations presented in Fig. 4, the pressure on the DW, $\partial\varepsilon(q)/\partial q$, depends on the pinning potential and the projection of the magnetic field H_y along the bend:

$$\partial\varepsilon(q)/\partial q = 0 \text{ for } q < 0 \text{(horizontal arm of the wire)}$$

$$\partial\varepsilon(q)/\partial q = -2H_yM_S\sin(q/R_c) \text{ for } 0 < q < \pi R_c/2 \text{ and } |q - q_i| > q_0$$

$$\partial\varepsilon(q)/\partial q = -2H_yM_S\sin(q/R_c) + 2V(q - q_i)/q_0 \text{ for } 0 < q < \pi R_c/2 \text{ and } |q - q_i| < q_0$$

$$\partial\varepsilon(q)/\partial q = -2H_yM_S \text{ for } q > \pi R_c/2 \text{(vertical arm of the wire)}$$

where $R_c = 3\,\mu$m is the radius of curvature of the bend, and q_i is the centre of the pinning potential. The experimental value for the depinning field, $H_y \approx 36$ Oe, is obtained for $q_i = 2.3\,\mu$m (corresponding to $\theta \approx 44°$). In our calculations, the DW is at its equilibrium position in the field when the current is turned on. We assume a rectangular pulse shape (zero rise and fall times).

Received 12 April; accepted 17 July 2006.

1. Malozemoff, A. P. & Slonczewski, J. C. *Magnetic Domain Walls in Bubble Material* (Academic, New York, 1979).
2. Berger, L. Exchange interaction between ferromagnetic domain wall and electric current in very thin metallic films. *J. Appl. Phys.* **55,** 1954–1956 (1984).
3. Berger, L. Possible existence of a Josephson effect in ferromagnets. *Phys. Rev. B* **33,** 1572–1578 (1986).
4. Slonczewski, J. C. Current-driven excitation of magnetic multilayers. *J. Magn. Magn. Mater.* **159,** L1–L7 (1996).
5. Berger, L. Emission of spin waves by a magnetic multilayer traversed by a current. *Phys. Rev. B* **54,** 9353–9358 (1996).
6. Grollier, J. *et al.* Switching a spin valve back and forth by current-induced domain wall motion. *Appl. Phys. Lett.* **83,** 509–511 (2003).
7. Vernier, N., Allwood, D. A., Atkinson, D., Cooke, M. D. & Cowburn, R. P. Domain wall propagation in magnetic nanowires by spin-polarized current injection. *Europhys. Lett.* **65,** 526–532 (2004).
8. Yamaguchi, A. *et al.* Real-space observation of current-driven domain wall motion in submicron magnetic wires. *Phys. Rev. Lett.* **92,** 077205 (2004).
9. Klaui, M. *et al.* Controlled and reproducible domain wall displacement by current pulses injected into ferromagnetic ring structures. *Phys. Rev. Lett.* **94,** 106601 (2005).
10. Klaui, M. *et al.* Direct observation of domain-wall configurations transformed by spin currents. *Phys. Rev. Lett.* **95,** 026601 (2005).
11. Yamanouchi, M., Chiba, D., Matsukura, F. & Ohno, H. Current-induced domain-wall switching in a ferromagnetic semiconductor structure. *Nature* **428,** 539–542 (2004).
12. Ravelosona, D., Lacour, D., Katine, J. A., Terris, B. D. & Chappert, C. Nanometer scale observation of high efficiency thermally assisted current-driven domain wall depinning. *Phys. Rev. Lett.* **95,** 117203 (2005).
13. Li, Z. & Zhang, S. Domain-wall dynamics driven by adiabatic spin-transfer torques. *Phys. Rev. B* **70,** 024417 (2004).
14. Tatara, G. & Kohno, H. Theory of current-driven domain wall motion: Spin transfer versus momentum transfer. *Phys. Rev. Lett.* **92,** 086601 (2004).
15. Thiaville, A., Nakatani, Y., Miltat, J. & Suzuki, Y. Micromagnetic understanding of current-driven domain wall motion in patterned nanowires. *Europhys. Lett.* **69,** 990–996 (2005).
16. Zhang, S. & Li, Z. Roles of nonequilibrium conduction electrons on the magnetization dynamics of ferromagnets. *Phys. Rev. Lett.* **93,** 127204 (2004).
17. Barnes, S. E. & Maekawa, S. Current-spin coupling for ferromagnetic domain walls in fine wires. *Phys. Rev. Lett.* **95,** 107204 (2005).
18. Saitoh, E., Miyajima, H., Yamaoka, T. & Tatara, G. Current-induced resonance and mass determination of a single magnetic domain wall. *Nature* **432,** 203–206 (2004).
19. O'Handley, R. C. *Modern Magnetic Materials: Principles and Applications* (Wiley and Sons, New York, 2000).
20. McMichael, R. D. & Donahue, M. J. Head to head domain wall structures in thin magnetic strips. *IEEE Trans. Magn.* **33,** 4167–4169 (1997).
21. Nakatani, Y., Thiaville, A. & Miltat, J. Head-to-head domain walls in soft nano-strips: a refined phase diagram. *J. Magn. Magn. Mater.* **290,** 750–753 (2005).
22. LLG Micromagnetic Simulator ⟨http://llgmicro.home.mindspring.com/⟩ (1997).
23. Park, J. P., Eames, P., Engebretson, D. M., Berezovsky, J. & Crowell, P. A. Imaging of spin dynamics in closure domain and vortex structures. *Phys. Rev. B* **67,** 020403 (2003).
24. Novosad, V. *et al.* Magnetic vortex resonance in patterned ferromagnetic dots. *Phys. Rev. B* **72,** 024455 (2005).
25. Shibata, J., Nakatani, Y., Tatara, G., Kohno, H. & Otani, Y. Current-induced magnetic vortex motion by spin-transfer torque. *Phys. Rev. B* **73,** 020403 (2006).

Acknowledgements We acknowledge financial support from DMEA.

Author Information Reprints and permissions information is available at www.nature.com/reprints. The authors declare no competing financial interests. Correspondence and requests for materials should be addressed to L.T. (lucthom@us.ibm.com) or S.S.P.P. (parkin@almaden.ibm.com).